

# DEVELOPMENT OF A CONTROL SYSTEM BASED ON EXPERIMENTAL DATA FOR SPACE CHARGE LENSES

S. Klaproth\*, C. Beberweil, M. Droba, O. Meusel, H. Podlech, B. Scheible, K. Schulte, K. Thoma, C. Wagner, Institute of Applied Physics (IAP), Frankfurt am Main, Germany

## Abstract

Space charge lenses use a confined electron cloud for the focusing of ion beams. The electron density gives the focusing strength whereas the density distribution influences the mapping quality of the space charge lens and is related to the confinement.

The major role of the electron density with respect to the focusing quality has been pointed out many times in the past [1, 2]. With an automated measurement system the radial light density profile, plasma stability and mean value of the electron density have been measured in respect to the confining fields and the pressure. The results are summarized in 3D-maps.

The theoretical model approximations for space charge lenses predicts high electron densities then measured. With the automated system the realistic 3D-maps can be considered instead of an approximation of a theoretical density including knowledge of the most stable electron cloud achievable within the parameter range of the lens.

The experimental results of the automated measurement system will be presented here and a concept of a control system for this type of space charge lenses will be explained.

## INTRODUCTION

The studied space charge lenses (Fig. 1) uses a positive potential and a magnetic field to trap electrons. The space charge of the confined electron can be used to focus ion beams. Therefore the electron density is crucial for the focusing strength. Under the assumption of a cold, homogeneous

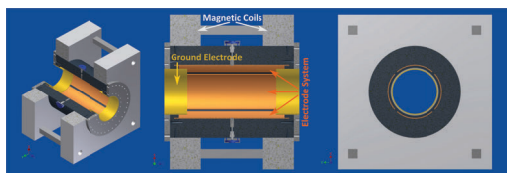


Figure 1: Scheme of investigated space charge lens.

distributed plasma column, the theoretical operation point is reached, if the longitudinal and radial confinement are equal concerning the electron density. Including the effects of neutralization background fraction  $f$  and the expansion of the plasma  $R_p$ , an operation function [1] can be described as:

$$\Phi_A(B_z, f) = \frac{eR_p^2 B_z^2}{8m_e} \left( 1 + 2 \ln \frac{R_A}{R_p} \right) (1 - f) \quad (1)$$

The corresponding electron densities can be derived through:

$$n_{e,r} = \frac{\epsilon_0 B_z^2}{2m_e} (1 - f) \quad n_{e,l} = \frac{4\epsilon_0 \Phi_A}{eR_p^2 (1 + 2 \ln(R_A/R_p))} \quad (2)$$

Where  $R_A$  is the radius of the anode. The theoretical model does not cover influences from gas types and pressure, which affects the temperature of the electron plasma [3] and influences the equilibrium of production and losses hence the plasma state and electron density. Further more, the filling degree  $\kappa$  of the lens is assumed to be much lower than the theoretical values. For this reason 3D-maps have been prepared for the electron density and parameters quantifying the plasma state. A 3D-map consists of units called 'charts'. A chart holds any measured configuration of the confinement parameters at a fixed pressure for one parameter. Instead of calculating the theoretical confinement parameters, the 3D-maps can be picked out for the needed electron density and the most suitable configuration so that the plasma is most stable.

## EXPERIMENTAL SETUP

The experimental setup (Fig. 2) was built and consists of an impulse spectrometer, a Faraday cup to detect the ion current of the emitted ionized gas and a liquid nitrogen cooled CCD Camera.



Figure 2: Experimental setup.

## Detection of the Electron Density

Residual gas ions are produced due to the ionization process within the lens volume. They are accelerated by the electric potential of the anode system partially reduced through the field of the confined electrons. Under the assumption of single ionization the energy of the ions is detectable (Fig. 3). From the difference of the anode potential and the measured energy of the ions (highest peak selected), the mean electron density is derived through Eq. 2.

## Evaluation of the Plasma Stability

The electrons are produced by ionization. The current of the emitted ions (Fig. 4) correlates strongly to the electron density [2]. If the plasma is stable, then the ion current is rather constant. Also instabilities like Diocotron instabilities can be detected this way. To evaluate the ion currents the

\* Stephan.Klaproth@stud.uni-frankfurt.de

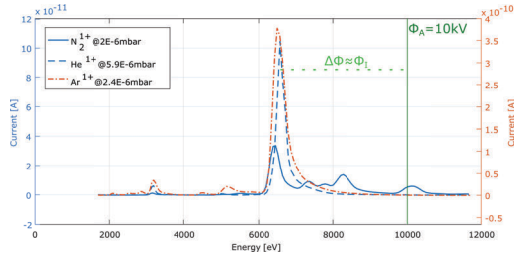


Figure 3: Energy spectra of  $He^{1+}$ ,  $N_2^{1+}$ ,  $Ar^{1+}$ -ions at operation point  $\Phi_A = 10$  kV,  $B_z = 8.1$  mT.

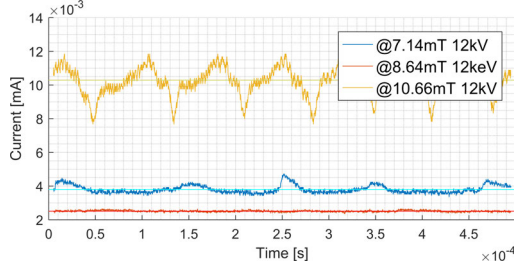


Figure 4: Detected ion current for different confinement settings (blue 7.14 mT 12 kV, red 8.64 mT 12 kV, blue 10.66 mT 12 kV).

A

coefficient of variation  $S_{CoV}$  is used:

$$S_{CoV} = \frac{\sigma_c}{\mu_c} \quad (3)$$

where  $\mu_c$  is the mean and  $\sigma_c$  the standard deviation of the measured current signal.

### Evaluation of the Radial Light Density Profile

The evaluation of the light density also uses the coefficient of variation. The center of light density within the region of interest (ROI) is derived. Afterwards, the radial and angular profiles are generated. Thereby we call the coefficients of variation on the radial profile Radial Deformation Factor ( $S_{RDF}$ ) Eq. (4) and on the angular profile Global Deformation Factor ( $S_{GDF}$ ) Eq. (5).

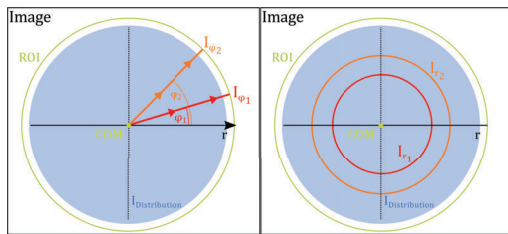


Figure 5: Scheme of GDF (left) and RDF (right) calculation.

$$S_{RDF} = \frac{\sum_{r=0}^R \left( \int_0^{2\pi} I(r, \varphi) d\varphi - \frac{1}{N} \sum_{r=0}^R \int_0^{2\pi} I(r, \varphi) d\varphi \right)^2}{\frac{1}{N} \sum_{r=0}^R \int_0^{2\pi} I(r, \varphi) d\varphi} \quad (4)$$

$$S_{GDF} = \frac{\sum_{\varphi=0}^{2\pi} \left( \int_0^R I(r, \varphi) dr - \frac{1}{N} \sum_{\varphi=0}^{2\pi} \int_0^R I(r, \varphi) dr \right)^2}{\frac{1}{N} \sum_{\varphi=0}^{2\pi} \int_0^R I(r, \varphi) dr} \quad (5)$$

Another way to rate the symmetry is gained by subtracting the integrated angular intensity by the opposite angular integrated intensity. The sum of the squared differences form the symmetry factor  $S_{rot,sqr}$  Eq. (6).

$$S_{rot,sqr} = \sum_{\varphi=0}^{2\pi} \left( \int_0^R I(r, \varphi) - \int_0^R I(r, \varphi + \pi) \right) \quad (6)$$

## EXPERIMENTAL RESULTS

The presented charts of the 3D-maps has been taken in steps of 0.5 kV and 0.5 mT with helium as residual gas. In all charts the theoretical operation function is plotted with neutralization background fraction of 0%, 5% and 10%. Any parameters quantifying the plasma state is best at zero.

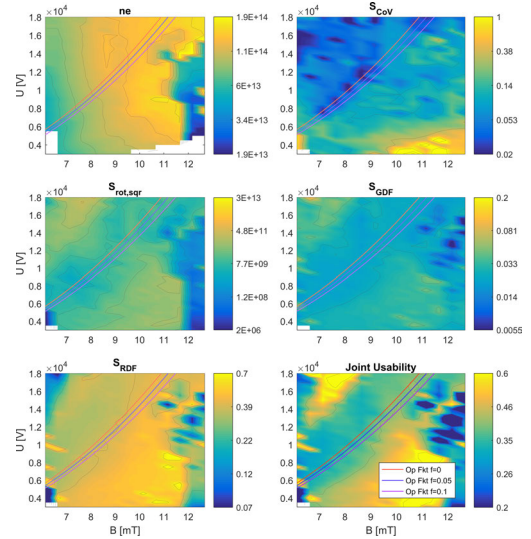


Figure 6: Measured electron density  $n_e$ ,  $S_{rot,sqr}$ ,  $S_{CoV}$ ,  $S_{RDF}$ ,  $S_{GDF}$  and joint usability for  $He 5.9 \times 10^{-6}$  mbar.

In Figure 6 the electron density rises constantly near the operation function. For magnetic fields above 11.5 mT and potentials below 16 kV the electron density collapses. Except for the region of collapsed electron density, any confinement configuration seems to be usable. For high magnetic fields, the plasma develops Diocotron instabilities [1]. That's why  $S_{CoV}$  returns greater values for higher magnetic fields especially at lower potentials. The best results are obtained close to the operation function according to  $S_{CoV}$ , but also for higher potentials the stability of the plasma is rather good. The parameter  $S_{rot,sqr}$  and  $S_{GDF}$  attest the region around the operation function best symmetry as well, while scores less aside of it. The values of  $S_{RDF}$  are best for higher potentials and low magnetic fields and worst for the opposite configuration. The joint usability shows the normed sum of all equally weighted parameters quantifying the plasma state presented here. The operation function with neutralization factor  $f = 0\%$  is rated very well. In addition, a shift of it to slightly higher potentials will operate well, too. A good mapping quality is expected for these configurations.

In Figure 7 the same measurement is presented at a higher residual gas pressure of  $17.7 \times 10^{-6}$  mbar helium. The electron density rises for most configurations. Especially close

to the operation function the slope increases until 9.5 mT, but saturates above. Also the plasma state is good along the operation function with neutralization factor  $f = 5\%$  up until 10.5 mT in accordance with  $S_{CoV}$ . Diocotron instabilities arise closer to the operation function compared to the lower pressure case. While high potentials configurations with magnetic fields below 9 mT getting more stable the saturated electron density region above 10 mT becomes more unstable. The clearly visible valley of the low pressure measurement is not present anymore for the parameter  $S_{rot,sqr}$ , but still the center region remains rather stable. The parameter  $S_{GDF}$  indicates good symmetry slightly below the operation function with  $f = 10\%$ , while  $S_{RDF}$  would suggest better performance for  $f = 0\%$ . The joint usability cannot lift out a special functional dependency for the focusing purpose. So lower pressure should always be preferred to maximize the mapping quality.

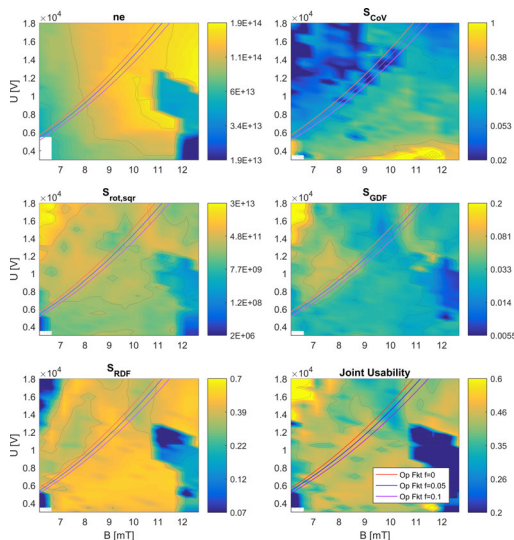


Figure 7: Measured electron density  $n_e$ ,  $S_{rot,sqr}$ ,  $S_{CoV}$ ,  $S_{RDF}$ ,  $S_{GDF}$  and joint usability for He  $17.7 \times 10^{-6}$  mbar.

## CONTROL SYSTEM CONCEPT

A control system for the adjustment of the focal length is currently under preparation. The following steps of the controlling process will be considered and further investigated. In the first step the theoretical needed electron density  $n_e$  is estimated with the user inputs focal length  $L$  and energy of the beam  $E_{beam}$  based on the thick lens approximation

$$L = k_G^{-1} \cot(k_G l) + l \quad (7)$$

with Gabor lens focusing constant  $k_G^2 = qen_e/4\epsilon_0 E_{kin}$ . Only solutions with  $l < L$  are valid [4].

The second step is to determine the confinement parameters to achieve the needed electron density. One option is to use the operation function under scaling with the mean  $\kappa$ . But as seen in Fig. 7 there are more stable confinements with expected better mapping quality aside the operation function. Therefore, the other option is to look at the 3D-maps instead of approximating the electron density. This way also other

influences like residual gas pressure and gas type can be taken into account.

Within the third step, the most suitable plasma state with the requested electron density reachable from the as-is state will be selected as target state. Generally, target states close to the operation function are easier to reach than aside of it due to the good plasma stability. Therefore, the potential and magnetic field of the confinement are adjusted in small steps along the operation function until the necessary magnetic field is established. Afterwards the potential is manipulated towards the target state. With online diagnoses, the plasma may be observed to detect the current electron density. These deliver information to adjust the confinement further and can be used to optimize the 3D-maps.

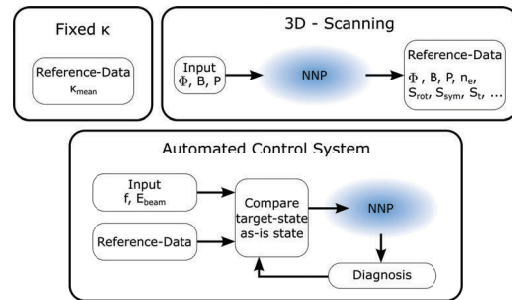


Figure 8: Control system concept.

## OUTLOOK

The 3D-maps have been measured and a general concept for a control system is designed. The next steps in the development will be implementing the automated control system into the control system MNDACS [5] and testing the performance with beam transport experiments at IAP. Also the influence of the beam current shall be studied, which has been observed at GSI Darmstadt (Fig. 9).

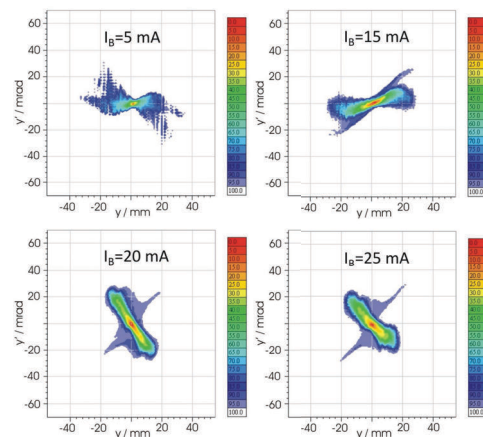


Figure 9: Influence of the ion current on the focusing performance. Confinement hold constant at  $\Phi_A = 9.5$  kV,  $B_z = 9.7$  mT,  $p = 1.3 \times 10^{-6}$  mbar.

## REFERENCES

- [1] K. Schulte, "Studies on the focusing performance of a gabor lens depending on nonneutral plasma properties," Ph.D. dissertation, Goethe University, Frankfurt a. M., Germany, 2014.
- [2] O. Meusel, "Focusing and transport of ion beams using space charge lenses," Ph.D. dissertation, Goethe University, Frankfurt a. M., Germany, 2006.
- [3] K. Schulte, "Untersuchung von Messmethoden zur Parameterbestimmung eines Nichtneutralen Plasmas," Diploma thesis, Goethe University, Frankfurt a. M., Germany, 2008.
- [4] B. Ivanov, "Plasma focusing devices in external programmed magnetic field," *Voprosy Atomnoj Nauki i Tekhniki. Yaderno-Fizicheskie Issledovaniya*, pp. 81–83, 1999.
- [5] S. Alzubaidi, O. Meusel, U. Ratzinger, K. Volk, and C. Wagner, "A control system for the FRANZ accelerator," *Proceeding of IPAC 2014, Dresden, Germany, THPRO103*, pp. 3134–3136, 2014.